2020 NA62 Status Report to the CERN SPSC

Abstract

The status of the NA62 experiment is reported. The ongoing activities on detectors and hardware are summarised, together with our plans for the restart of data taking in 2021. Results of the $K^+ \to \pi^+ \nu \bar{\nu}$ analysis based on the 2017 data set are presented. The status of the analysis of the data collected is reviewed in detail. Highlights of rare and forbidden decay analyses and exotic searches are also briefly discussed.

1 Introduction

Since the previous report in April 2019, the NA62 experiment analyzed the data collected in 2017, achieving world-leading single event sensitivity for the $K^+ \to \pi^+ \nu \bar{\nu}$ decay. The 2017 $K^+ \to \pi^+ \nu \bar{\nu}$ result was presented at the International Conference KAON2019 and at a CERN EP Seminar in Autumn 2019. The 2017 data also allow NA62 to achieve the best sensitivity on the search for the $\pi^0 \to invisible$ decay. These results are being prepared for publication.

In October 2019 the experiment submitted Addendum 1 to P326 to the SPSC, proposing the continuation of the physics programme after LS2, and the first year of data taking has been approved. The FRC of November 2019 approved the budget for 2020, including a 4th GTK station, allowing us to ramp up the preparation for data taking after LS2.

During 2019 and 2020 the $K^+ \to \pi^+ \nu \bar{\nu}$ analysis strategy has been focused on improving the signal sensitivity. The experiment has invested significant resources to improve the Monte Carlo simulation. In addition a quantitative data and Monte Carlo comparison of the upstream background has been performed and ways to reduce this background for future data taking have been identified.

This report offers a summary of the $K^+ \to \pi^+ \nu \bar{\nu}$ analysis based on 2017 data, and presents new estimates in terms of expected numbers of signal and background events for the data collected in 2018. Thanks to a substantial analysis effort, several additional physics analyses are ongoing, spanning precision measurements, searches for lepton number and flavour violating processes, and searches for exotic long lived particles.

The document is structured as follows: Sections 2, 3 and 4 summarise the ongoing activities on the hardware and the data quality and simulation; the $K^+ \to \pi^+ \nu \bar{\nu}$ analysis on the 2017 data and an update of the 2018 data are described in Section 5; Sections 6 and 7 report current highlights of rare/forbidden decays and exotic searches, respectively. Finally, the list of recent publications is presented in Section 8.

2 Status of the detector and on-going activities

A description of the detector can be found in [1] and a schematic is shown in Fig 1.

The major maintenance operation during LS2 concerns the vacuum system. In particular, the cryo-pumps of the vacuum system will undergo a thorough check and replacement of key components, performed by an outside company, by Autumn 2020. This will allow efficient operation of the vacuum system in the decay volume until LS3. The water cooling for the LKr will be switched on in April 2020, to allow for tests of the readout system.

The level of the liquid krypton in the LKr detector has been stable since the summer of 2017 and there is no urgent need to top up the liquid krypton at this point. Nevertheless, about 400 litres of liquid krypton were bought in 2017 and they will be added to the krypton storage dewar during 2020. A dedicated device has been built to validate the purity of the krypton by measuring the lifetime of the drift electrons. The first tests of this new device were carried out in the summer of 2018 and were not conclusive due to high noise level in the readout. In order to improve the signal-to-noise ratio, the front-end electronics has been modified. The final validation of the new system was carried out during a second test in the fall of 2019. The measurement validated both the purity of the krypton and the device itself. At present the plan is to transfer the krypton to the storage dewar before summer.

Improvements to the radiation shielding were made prior to the 2018 data taking. The electronics racks for the KTAG, CHANTI and GTK cooling stations were equipped with additional concrete blocks to decrease the number of single event upsets (SEUs). Neutron shielding (boron carbide) was added to electronics racks of the KTAG. Details can be found in the 2019 SPSC report [2].

In order to reduce the upstream background affecting the $K^+ \to \pi^+ \nu \bar{\nu}$ analysis, the beam layout upstream of the decay volume will be modified. The main modifications are:

- an optimized achromat layout;

- a 4th GTK station;

- a new veto–counter system around the beam pipe

The new layout (see Fig. 2) has been simulated extensively, and the upstream background is expected to be reduced by a factor 2–3. The position of the different beam components and vacuum sections in the modified beam lime have been determined; in order to start the detailed design and the update of the CAD model, an Engineering Change Request (ECR) which includes the beam layout with the new vacuum sections and the modifications to the GTK cooling station has been launched. Once the detailed CAD model is available, the manufacturing of the components and the rearrangement of the achromat will start. The plan is to complete the installation before the end of 2020, including the installation of GTK4. The fourth cooling line for GTK4 and the modifications to the cooling station are expected to be completed by October 2020. The purpose of the veto-counter system placed before the final collimator is to detect charged pions and photons from upstream kaon decays. Simulations have resulted in a conceptual design based on small scintillator-lead-scintillator modules read out by fast photomultipliers. The exact size and segmentation are under study and will be optimized by taking also into account both the expected particle rates and the results of a prototype test scheduled for 2020.

2.1 Sub-Detectors

The annual maintenance and intervention on the detector include: the replacement of ageing SiPM in CHANTI; the recovery of dead/noisy channels in KTAG and LAVs; the installation of the LAV internal calibration system, allowing monitoring of the detector without beam during LS2; the refurbishment of the shaper boards in MUV1,2 and replacement of ageing photomultipliers in MUV2; the replacement of the RICH HV mainframes (two out of four were replaced already in April 2019), given that maintenance of the old type is no longer guaranteed by the manufacturer. The RICH neon quality is routinely monitored and the detector will be kept as it is until the start of data taking in 2021; if needed one full neon fill is available.

As part of the new upstream beam layout, the GTK has been extended from three stations to four. Based on previous experience, 8 detector modules per year (4 in the beam + 4 spare) are needed. Taking into account some contingency in fabrication and operation, the fabrication of 16 new modules is planned to cover data taking after LS2. Orders for all the required parts have been placed and the detectors required for the start-up in 2021 have been assembled. Our present fabrication rate is based on six detector modules per year, and the detector modules (including spares) should be completed in 2022.

A new high-voltage connector for the LKr detector has been developed in collaboration with LEMO after repeated vacuum leaks in the high-voltage feedthroughs. At present there are no apparent leaks and the replacement of connectors will only happen if there are new leaks. Spares are available for all parts of the calorimeter's read out.

The HASC has been also proven to be effective as a photon veto complementary to the LAV, LKr, IRC and SAC calorimeters, giving an additional 30% background reduction as seen in the $K^+ \to \pi^+ \nu \bar{\nu}$ analysis of 2016 data and confirmed with 2017 data. Given the success of the HASC as photon veto, we plan to duplicate it in a symmetrical position with respect to the beam axis, to further increase the π^0 rejection. The nine modules for the second HASC station
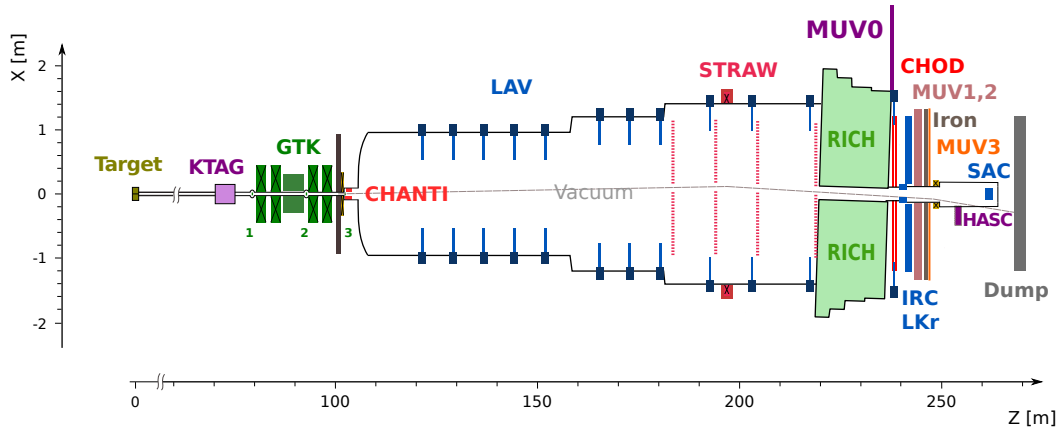
Figure 1: Layout of the NA62 experiment. KTAG: differential Cherenkov counter; GTK: Si pixel beam tracker; CHANTI: ring stations of scintillator bars; LAV: lead glass ring calorimeters; STRAW: straw magnetic spectrometer; RICH: ring imaging Cherenkov counter; MUV0: off-acceptance plane of scintillator pads; CHOD: planes of scintillator pads and slabs; IRC: inner ring shashlik calorimeter; LKr: electromagnetic calorimeter filled with liquid Krypton; MUV1,2: hadron calorimeter; MUV3: plane of scintillator pads for muon veto; HASC: near beam lead–scintillator calorimeter; SAC: small angle shashlik calorimeter. In the layout, the final fixed collimator installed in 2018 is visible, between GTK and CHANTI.
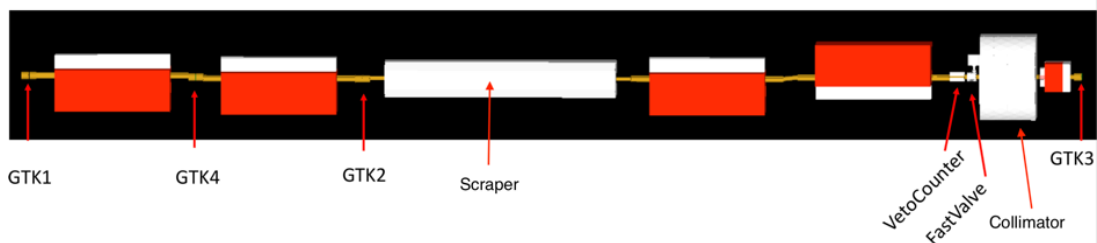
Figure 2: Schematic layout of the new achromat as seen in the simulation.

have been procured and the support structure is completed. The modules will be installed and integrated before the end of 2020.

A new hodoscope (ANTI0) against the background present in dump mode searches will be installed for the next data taking, at the entrance of the fiducial volume (see section 7).

In April 2019, the EN/EA group identified a CEDAR that could be used as an operational spare, to mitigate the risk of relying on a instrument which is so far unique. The CEDAR-KTAG detector is absolutely essential for the $K^+ \to \pi^+ \nu \bar{\nu}$ analysis, since without the time and identification of the kaon it is impossible to achieve sufficient background rejection. Inspection and systematic studies of the existing optical system of the spare have started. Given the reduction in background expected from the changes in the beam line changes and the additional HASC module, further improvement in the signal to background ratio may result from the use of H_2 in the CEDAR (part of the original experiment design) which minimizes the material crossed by the beam. Using hydrogen instead of nitrogen would also help to reduce radiation-induced effects in the area. While the use of H_2 would be possible with the current CEDAR, the loss of light with respect to N_2 makes its use impossible when considering that the current optics is not optimised for H_2. Hence an effort is on-going to identify the characteristics of the optical elements best suited for H_2 use and their tolerances. Plans for testing and commissioning the device with beam after LS2 are being developed. Once the CEDAR-H_2 is successfully commissioned, the existing CEDAR-N_2 will be kept as a fully operational spare.

2.2 TDAQ

In the spirit of further improving the data taking efficiency and the trigger performance, the main focus of TDAQ activity has been to address the issues detected during the 2018 run. This was done by performing a series of dry runs with the readout exercised with noise or pulser triggers. The on-going investigations are detailed below.

The L0 trigger processor (L0TP) showed two issues: the onset of oscillations in the trigger rate from burst to burst at high intensity and the non-uniform population of the number of triggers across the 6.4 μs time window employed to pack the primitive data. Since the tests performed by injecting signals to the TDC input didn't reproduce the problem, the development of a more realistic test system was necessary. The new emulator, called TRIBE (TRIgger Burst Emulator), is capable of storing real trigger primitives (collected in parallel during the data taking) in its memory and sending them, with the original timing structure, to the L0TP. TRIBE will be able to identify and debug the problems encountered during the 2018 high-intensity run. In addition, an unexplained low trigger efficiency during the beam dump runs was found to be caused by a bug in the trigger firmware where, when merging control and reference primitives, the last primitive of one of the two chains was lost. This problem was shown to have been fixed in 2019 during one of the test runs, with an appropriate configuration of the pulser boards. The fix was then verified with the first version of the TRIBE emulator, demonstrating the functionality of the emulator itself.

The existing readout system for the GTK exhibited rate limitations during nominal-intensity tests, and an intervention to identify and improve the relevant part of the firmware is foreseen for early Summer 2020.

A regular interaction with the company CAEN (author of the CREAM readout firmware) has started, in order to solve some features of the LKr readout seen during 2017 and 2018 runs. The main aims are to eliminate the "swap" problem (namely the swap between the values of the first 16 channels with the other 16) at initialization, and to fix a problem in the multi-event packing (implemented to reduce the number of packets on the network) whereby packets are sent with a sizable frequency to the wrong farm PCs. It is expected that a new version with a first fix will be available in May 2020, and will be tested at NA62 on the entire LKr readout,

once the cooling in ECN3 is switched on.

In preparation for data taking in 2021, a number of improvements have been carried out or are in progress for the overall TDAQ system:

- It was found in 2018 that the back-pressure signal (CHOKE), generated by the readout boards when the FIFO are full, is important to reduce the losses due to instantaneous intensity fluctuations of the beam. The hardware to collect and merge together all the CHOKE signals from the readout boards was reviewed and its reliability improved.

- The L0 calorimeter trigger will be enhanced with information from the MUV1/2 hadronic calorimeters, making available a total calorimetric energy condition, and a di-electron condition, based on topological information of electromagnetic clusters. These new conditions will be used to improve the selectivity of triggers with two electrons in the final state. The information used for these trigger conditions (i.e. energies and positions of the clusters) will also be fully readout and used by the L1 trigger, to achieve additional rejection.

- The firmware for the existing pattern-generating cards to pulse the TDC system will be upgraded, to allow for better and more realistic testing.

- Further investigation and testing of the GPU-based L0 trigger system, which was deployed and parasitically used for the RICH during 2018, is on-going. A trigger condition on RICH rings is intended to improve the selectivity of L0 triggers for rare kaon decays with an electron in the final state.

- A thorough study of sources of inefficiencies in the whole TDAQ system was undertaken, exploiting all the available recorded information. The study indicates that several sources contribute, and identified a few pieces of missing information which will be recorded to fully monitor all sources of downtime. The study also identified which information should be monitored to allow a faster reaction by the shift crew.

In preparation for the 2021 data taking, a list of actions has been defined to improve the reliability and the monitoring of the readout. The online monitor program will be updated to be faster in processing and presentation. A refurbishment campaign of service PCs is on-going. An improvement of the PCFarm system is under consideration. A small number of TEL62 and TDCB cards has been produced in 2019, both to increase the number of available spares and to accommodate the readout of new units, for which the cables will be ordered soon.

To profit from advances in technology and maintain good performances at higher beam rate, two new items are being developed:

- A replacement for the L0 processor (L0TP+) based on more modern technology. The existing L0TP firmware has already been deployed onto the new hardware, and laboratory tests are starting. The new system, initially run in parallel with the existing L0TP, will be fully validated with beam and will eventually be substituted for the current one.

- A prototype FPGA-based TDC system, capable of standing higher rates with no dead time, that is going to be readout directly into PCs using ATLAS Felix boards. This system will be fully tested and validated with beam in 2021, and eventually will be used for high-rate detectors such as KTAG.

3 Data Quality and Data Processing

Since April 2019 efforts have been concentrated on improving the calibration procedures of several detectors (see details below), and on simplifying and making more efficient the processing

of the raw data. This optimization, together with improvements in the processing system itself, reduces the processing time of all physics data taken in 2016-2018 by a factor of two.

A major change was the introduction of the so-called "Slim Persistency". By purging redundant information and reducing the storage size of all variables, a reduction of about a factor three was achieved in the output files for user analysis. All the processed data now occupy about 1.8 PBytes for the full 2016-8 data set.

The full 2018 data set was processed for the first time in the second half of 2019, and the results indicated the need of improvements in the calibrations. The 2018 data set is currently being re-processed with the latest software revision, which include:

- Improved evaluation of the GTK timing corrections

- Improved evaluation of the GTK x-y alignment

- Improved CHOD timing calibration procedure

- A new energy calibration of the LKr using photons from π^0 decays

- An offline determination of the luminosity (kaon flux) on a run-by-run basis improving on a procedure used online during data taking

- Processing of the High Level Trigger (HLT) information

Improvements to the processing system itself include the removal of all the dependencies in using ATLAS resources (since the system is based on that of ATLAS); the use of the CentOS7 operating system; and improved error handling. In preparation for the 2021 data taking, the necessary changes for the new CTA (CERN Tape Archive) system (replacing Castor) are being implemented, and the Online Monitoring system is being improved, preparing for an even faster feedback system (quasi-online) for the newly acquired data.

With our current allocation of 4 PByte of EOS space we can keep all the files for user analysis, have enough temporary space during the processing of the data, and have the newly needed EOS buffer space for the CTA operation, both for recalling data from tapes for processing and for writing the acquired raw data to CTA. The space available is expected to be sufficient for the 2021 data taking. However, an increase of about 1 PByte for every year of additional data taking until 2024 is needed, eventually reaching a total quota of 8 PBytes in 2025. We would like to express our gratitude to the IT Department for their support and expertise in assisting the needs of the experiment, and in particular to Xavier Espinal and Bernd Panzer-Steindel, for the excellent support and services provided to us.

4   MC simulation

Since April 2019, considerable efforts have been directed towards assessing the validity and precision of the NA62 Monte Carlo simulation package, including the creation of a dedicated working group. The aim is to identify areas where improvement is needed, especially regarding data/simulation comparison. Specific challenges are the event and track-pileup treatment, and an efficient biasing procedure to allow for the production of large MC samples of ultra rare events.

A major improvement recently implemented is an event-overlay method that is applied consistently to all detectors. The previous pile-up-generator was applied on a case-by-case basis to detectors at post-reconstruction level, and led to a partial treatment of the overlays. The new overlay of multiple Monte Carlo events at reconstruction level is systematically applied equally to all detectors, significantly improving the simulation-data agreement.

The emulation of the L0 trigger was added and applied at reconstruction level, allowing meaningful comparison of trigger effects between data and simulation. Similarly, the software L1 trigger can now be executed during the reconstruction of MC events, thanks to the development of a conversion algorithm that translates MC information into data-like format. In the case of the $K^+ \to \pi^+ \nu \bar{\nu}$ analysis this upgrade plays a minor role, since all trigger related effects are determined with data. Still, these developments are crucial for other analyses and also offer the opportunity to study the efficiency and rejection performance of future trigger lines.

Another improvement of our simulation package has been the introduction of better magnetic field maps of the NA62 beamline, recently made available by the EN/EA and TE/MSC groups [3]. Thanks to these detailed maps, it has been possible to simulate upstream events samples that have both aided the $K^+ \to \pi^+ \nu \bar{\nu}$ analysis and the study of the beamline modifications planned for 2021, including optimization studies for the new veto counter.

Ongoing projects are:

- the inclusion of the beam particle simulation as provided by the EN/EA group using the G4 beamline software. As a result, a realistic description of the beam and background particles is obtained. Its validation is ongoing, while the framework is ready.

- the development of event biasing techniques (for example hadronic interactions in GTK3), as well as the design of a fast simulation with shower databases for downstream detectors, in order to significantly improve the speed of simulation for ultra-rare events.

5   Status of the $K^+ \to \pi^+ \nu \bar{\nu}$ analysis

The $K^+ \to \pi^+ \nu \bar{\nu}$ analysis of the 2017 data has been presented at KAON2019 and is detailed in section 5.1; the results will soon be submitted for publication.

With this result, NA62 is the first experiment worldwide to reach a sensitivity on single π^+ detection of few 10^{-11}, reaching the best up–to–date result on the $K^+ \to \pi^+ \nu \bar{\nu}$ decay. The strategy to achieve such a challenging goal was to firstly push for the highest level of background rejection, without fine tuning of the signal sensitivity. This approach led NA62 to pin down the unexpected background from upstream K^+ decays. To keep it under control it was necessary to make strong cuts, reducing the signal acceptance to a few percents, significantly smaller than originally foreseen.

Thanks to the in–depth study of the $K^+ \to \pi^+ \nu \bar{\nu}$ done so far, the analysis can now move to the phase of optimization, with the goal to increase the signal efficiency, while keeping the background under control. To this end, the 2017 data was used to optimize the analysis, as described in section 5.2. The modifications and improvements achieved until now have been then applied to the 2018 data, as detailed in section 5.3. Finally, the prospects and plans using a full optimization of all aspects of the analysis for 2021 data and beyond are presented in section 5.4.

5.1   Results from the 2017 data set

The results shown in this subsection represent the NA62 result on 2017 data, and will soon be published.

In 2017 the SPS P42 beam line has delivered about 1.9×10^{12} protons per pulse, corresponding to about $450\,\mathrm{MHz}$ of particles in the GTK detector. Information from CHOD, RICH, MUV3 and LKr are used online to issue L0 trigger conditions [4]. Software-based variables from KTAG, CHOD, LAV and STRAW provide higher level trigger requirements. Data for $K^+ \to \pi^+ \nu \bar{\nu}$ analysis are taken concurrently with downscaled samples of data for other rare decays studies, and a minimum bias sample.
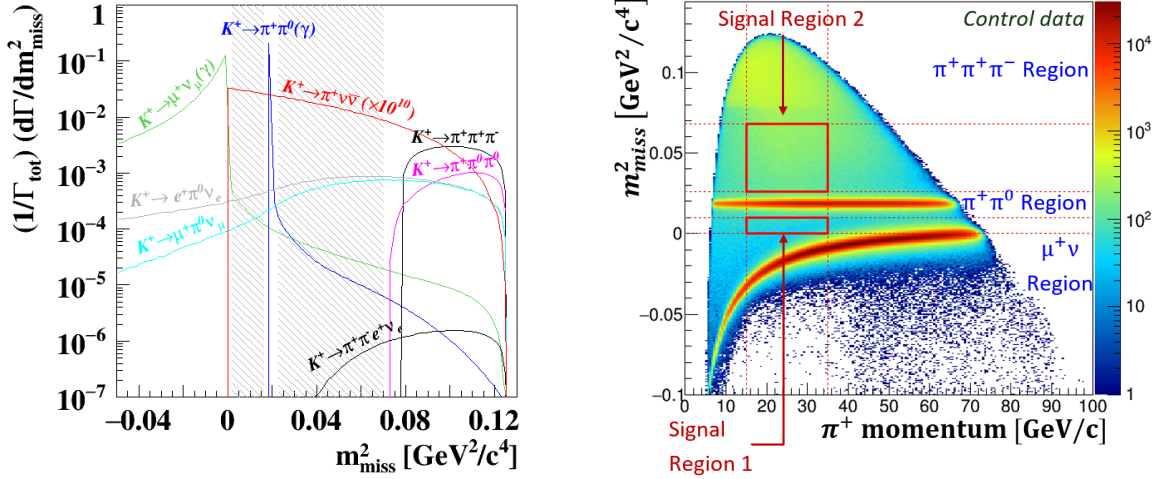
Figure 3: **Left**: m^2_{miss} of K^+ decays relevant to the $K^+ \to \pi^+ \nu \bar{\nu}$ measurement. The m^2_{miss} is computed under the hypothesis that the charged particle in the final state is a π^+. The signal (red) is multiplied by 10^{10} for visibility. The dashes areas denote the regions where to search for signal. **Right**: m^2_{miss} versus π^+ momentum of selected K^+ decays on minimum bias data. The signal regions 1 and 2 and the three background regions are also indicated.

The signature of a $K^+ \to \pi^+ \nu \overline{\nu}$ decay is a K^+ in the initial state and a π^+ with missing energy in the final state. The main kinematic variable is $m^2_{miss} \equiv (P_K - P_\pi)^2$, where P_K and P_π are the 4-momenta of the K^+ and π^+, respectively. The m^2_{miss} of the signal is broadly distributed, as shown in Fig. 3 (left). The search for the signal is performed in two intervals of the m^2_{miss} spectrum either side of the $K^+ \to \pi^+ \pi^0$ peak.

Possible backgrounds are: $K^+ \to \pi^+ \pi^0$, $K^+ \to \mu^+ \nu$ and $K^+ \to \pi^+ \pi^+ \pi^-$ entering signal regions through non–gaussian resolution and radiative tails of the m^2_{miss}; $K^+ \to l^+ \pi^0 \nu_l$ decays and rare processes like $K^+ \to \pi^+ \pi^- e^+ \nu$, which are broadly distributed across the signal regions; events mimicking $K^+ \to \pi^+ \nu \overline{\nu}$ originating along the beam line via inelastic interactions of beam particles with the material; K^+ particles decaying before entering the fiducial volume defined as downstream of the last station of the GTK (GTK3). Each source of background requires different rejection procedures, depending on the kinematics and on the type of charged particle in the final state. The estimation of the expected background is done separately for each process. A blind analysis procedure has been adopted, with signal and control regions kept masked until the evaluation of the signal and background is complete.

The selection of the $K^+ \to \pi^+ \nu \overline{\nu}$ decays (briefly denoted "PNN selection") proceeds as detailed below. A STRAW track associated to signals in RICH, LKr and CHOD defines a π^+. A signal in KTAG associated to a GTK track defines a K^+. The K^+ is coupled to the π^+ by matching in time and space the corresponding tracks. Selection criteria applied to the reconstructed decay vertex define the fiducial decay region downstream of GTK3. Additionally, events are rejected if the π^+ track originates from the beam aperture of the final collimator. Fig. 3 right shows the distribution of the selected events in the (m^2_{miss}, p_{π^+}) plane. Here p_{π^+} is the π^+ momentum. The m^2_{miss} is computed using the K^+ and π^+ momenta measured in GTK and STRAW assuming the K^+ and π^+ masses, respectively. This plane defines two signal regions, termed Region 1 and 2, and three background regions mostly populated by $K^+ \to \pi^+ \pi^0$, $K^+ \to \mu^+ \nu$ and $K^+ \to \pi^+ \pi^+ \pi^-$ decays. The analysis is restricted to $(15, 35)\,\mathrm{GeV}/c$ π^+ momentum, leaving at least 40 GeV of extra energy to veto background events. The selection proceeds

Table 1: *Expected signal and background events. $K^+ \to \pi^+\pi^0(\gamma)$ IB and $K^+ \to \mu^+\nu_\mu(\gamma)$ IB include also the contribution from the inner Bremsstrahlung radiation.*

Process	Expected events
$K^+ \to \pi^+\nu\bar{\nu}$	$2.16 \pm 0.12_{syst} \pm 0.26_{ext}$
$K^+ \to \pi^+\pi^0(\gamma)$ IB	$0.29 \pm 0.03_{stat} \pm 0.03_{syst}$
$K^+ \to \mu^+\nu_\mu(\gamma)$ IB	$0.11 \pm 0.02_{stat} \pm 0.03_{syst}$
$K^+ \to \mu^+\nu_\mu\,(\mu^+ \to e^+ decay)$	$0.04 \pm 0.02_{syst}$
$K^+ \to \pi^+\pi^-e^+\nu_e$	$0.12 \pm 0.05_{stat} \pm 0.03_{syst}$
$K^+ \to \pi^+\pi^+\pi^-$	$0.02 \pm 0.02_{syst}$
$K^+ \to \pi^+\gamma\gamma$	$0.005 \pm 0.005_{syst}$
$K^+ \to l^+\pi^0\nu_l\,(l = e^+, \mu^+)$	negligible
Upstream background	$0.9 \pm 0.2_{stat} \pm 0.2_{syst}$
Total background	$1.5 \pm 0.2_{stat} \pm 0.2_{syst}$

with the π^+ identification using the calorimeters and the RICH, achieving a suppression of eight orders of magnitude for muons. Events with photons are rejected by exploiting the time coincidence between the π^+ and possible signals in LAV, LKr, IRC or SAC. Selection criteria based on activity in CHOD and STRAWs are used to reject photons interacting with the material upstream of the LKr. The π^0 detection inefficiency is about 1.4×10^{-8}, measured on data. The above criteria are also effective against decays like $K^+ \to \pi^+\pi^+\pi^-$ and $K^+ \to \pi^+\pi^-e^+\nu$. Finally events are excluded if CHANTI signals in time with the π^+ or extra hits in at least 2 GTK stations are present. The $K^+ \to \pi^+\nu\bar{\nu}$ candidates are defined as those events in Regions 1 and 2 that pass the selection criteria described above.

The number of expected Standard Model (SM) $K^+ \to \pi^+\nu\bar{\nu}$ events, $N_{\pi\nu\nu}$, is estimated as:

$$N_{\pi\nu\nu} = N_{\pi\pi}\epsilon_{trig}\epsilon_{RV}\frac{A_{\pi\nu\nu}}{A_{\pi\pi}}\frac{BR(\pi\nu\nu)}{BR(\pi\pi)}. \tag{1}$$

Here $N_{\pi\pi}$ is the number of $K^+ \to \pi^+\pi^0$ decays selected from minimum bias data. The selection is the same as the PNN one, except that the photon rejection cuts not applied and the m^2_{miss} is required to be compatible with $m^2_{\pi^0}$. The symbol ϵ_{trig} denotes the efficiency of the trigger used to collect data for the $K^+ \to \pi^+\nu\bar{\nu}$ analysis. ϵ_{RV} denotes the random veto efficiency, defined as 1 minus the probability for a signal event to be randomly rejected by the photon veto conditions. Both ϵ_{trig} and ϵ_{RV} are measured on data. The random veto efficiency in 2017 is about 64% on average, but depends on the instantaneous beam intensity measured event–by–event from the activity in the time sidebands of the GTK. The symbols $A_{\pi\nu\nu}$ and $A_{\pi\pi}$ denote the geometrical and selection acceptances for signal and $K^+ \to \pi^+\pi^0$ decays, estimated from Monte Carlo simulations. Finally, $BR(\pi\nu\nu)$ and $BR(\pi\pi)$ are the SM predicted and the measured branching ratios of the $K^+ \to \pi^+\nu\bar{\nu}$ and the $K^+ \to \pi^+\pi^0$ decays [5], respectively. The number $N_{\pi\nu\nu}$ is evaluated in four bins of π^+ momentum. The efficiencies ϵ_{trig} and ϵ_{RV} are combined, taking into account their dependence on the instantaneous beam intensity.

By definition, the single event sensitivity (SES) is equal to $BR(\pi\nu\nu)/N_{\pi\nu\nu}$. The measured SES is $(0.389 \pm 0.021_{sys}) \times 10^{-10}$ corresponding to $N_{\pi\nu\nu} = 2.16 \pm 0.12 \pm 0.26_{ext}$. The systematic uncertainty on SES is mostly due to the evaluation of ϵ_{trig} and $A_{\pi\nu\nu}$. The external uncertainty of $N_{\pi\nu\nu}$ comes from the theoretical error on $BR(\pi\nu\nu)$. The sensitivity achieved corresponds to about 2×10^{12} K^+ decays analyzed. The statistics collected in 2017 have allowed NA62 to
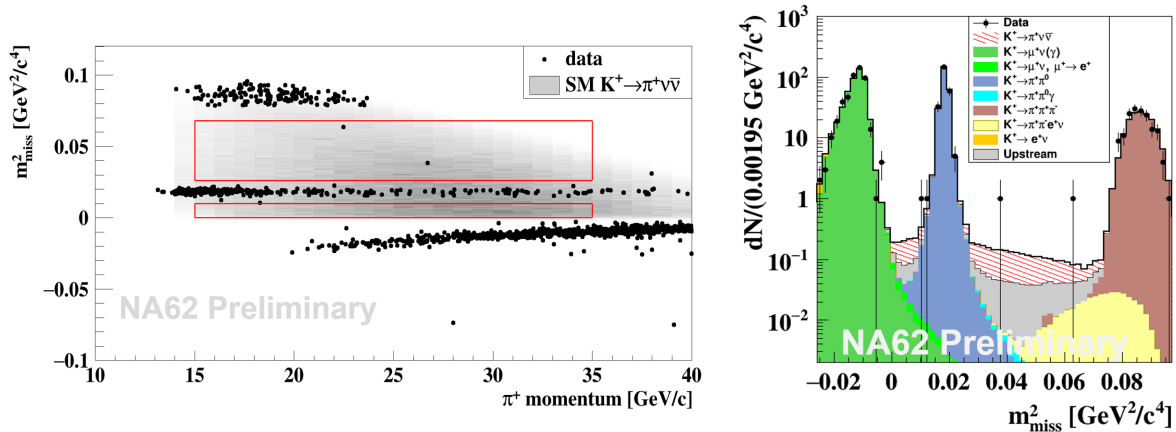
Figure 4: **Left**: m^2_{miss} *versus* π^+ *momentum of the events passing the* $\pi\nu\nu$ *selection. The red boxes indicate the signal Regions 1 and 2. The shadowed grey area represents the distribution of simulated* $K^+ \to \pi^+\nu\bar{\nu}$ *events.* **Right**: m^2_{miss} *for the events in the* $(15, 35)\,GeV/c\,\pi^+$ *momentum passing the* $\pi\nu\nu$ *selection, compared to the expected signal and background. Both data and Monte Carlo samples are used to derive the shape of the* m^2_{miss} *for the various backgrounds.*

achieve the best up–to–date single event sensitivity for $K^+ \to \pi^+\nu\bar{\nu}$.

Table 1 summarizes the expected SM signal and background events passing the $\pi\nu\nu$ selection for Region 1 and 2 together. The sources of background can be divided into: K^+ decays happening in the fiducial volume; and upstream background events, with π^+s originated from decays or interactions of K^+s occurring upstream of the final collimator. Samples of background–enriched data are used to validate the simulation down to the $K^+ \to \pi^+\nu\bar{\nu}$ SES. The agreement between expected and observed background events in suitable control regions validates the procedures of background estimation.

The evaluation of the $K^+ \to \pi^+\pi^0$ and $K^+ \to \mu^+\nu$ background relies on the assumption that π^0 and μ^+ rejection are independent from the m^2_{miss} cuts defining the signal regions. Kinematically unbiased samples of $K^+ \to \pi^+\pi^0$ and $K^+ \to \mu^+\nu$ events selected on minimum bias data provide a measurement of the probability for these decays to enter the signal regions as a consequence of a mis–reconstructed kinematics. The expected background stems from this probability and the number of events surviving the PNN selection in the corresponding m^2_{miss} background regions. Corrections are applied to account for correlations between kinematic and π^0 and μ^+ rejections using both simulations and data. A similar procedure is adopted to assess the $K^+ \to \pi^+\pi^+\pi^-$ background. The estimation of the other backgrounds from K^+ decays relies on Monte Carlo simulations normalized to $K^+ \to \pi^+\pi^0$ decays, as for the signal.

For upstream events, a lone π^+ can enter the region downstream through the beam aperture of the final collimator, with the collimator itself preventing the detection of the extra energy produced concurrently with the π^+. The π^+ mimics a signal event if accidentally matched to a random beam particle. In addition to this, the direction of the π^+ must be mis–reconstructed to create a fake decay vertex in the fiducial volume and to trace back the π^+ outside the beam aperture of the final collimator. The determination of the upstream background exploits the probability of an accidental matching of a π^+ to a random beam track and the total number of events surviving the PNN selection, with the criteria of $K^+ - \pi^+$ association inverted.

The analysis described above is repeated in the $(35, 40)\,GeV/c\,\pi^+$ momentum range. In this case about 0.62 background and 0.13 signal events are expected in the m^2_{miss} ranges equivalent

11

to Regions 1 plus 2, while 1 event is observed.

Fig. 4 left shows the m^2_{miss} versus p_{π^+} distribution of the events passing the PNN selection after the analysis of the 2017 data. Two events are observed in the signal regions, in agreement with the 2.16 signal and 1.5 background events expected. The observed events in the $(15, 35)\,\mathrm{GeV/c}$ π^+ momentum region compared with the expected backgrounds are shown in Fig. 4 right.

Adding the NA62 result on $K^+ \to \pi^+ \nu \bar{\nu}$ obtained from the analysis of the 2016 data [6], the overall SES is $(0.346 \pm 0.017) \times 10^{-10}$, 1.65 ± 0.31 background events are expected and 3 signal candidates observed. Using the CLs method [7], a simple event counting approach gives a preliminary observed upper limit $BR(K^+ \to \pi^+ \nu \bar{\nu}) < 1.85 \times 10^{-10}$ at 90% CL. The corresponding 90% CL expected upper limit is 1.32×10^{-10}. This result translates into a 90% CL Grossman–Nir limit [8] on the SM $K_L \to \pi^0 \nu \bar{\nu}$ branching ratio equal to 8.14×10^{-10}.

5.2 Towards the 2018 result: analysis optmization

The analysis of the 2017 data described in section 5.1 aimed to reach the highest level of:

1. muon rejection over all the phase space;

2. suppression of the $K^+ \to \pi^+ \pi^+ \pi^-$ background, by exploiting the kinematics of the detected π^+;

3. rejection of the upstream background, by removing events geometrically consistent with a charged pion originated upstream along the beam line and entering the fiducial volume due to lack of shielding

4. photon rejection.

The result of this analysis shows that:

- the μ^+ background in Region 2 is negligible with respect to that from upstream events, $K^+ \to \pi^+ \pi^0$ and $K^+ \to \pi^+ \pi^- e^+ \nu$ decays;

- the $K^+ \to \pi^+ \pi^+ \pi^-$ background is negligible;

- the geometrical cuts (applied to tracks extrapolated to the longitudinal position of the final collimator), necessary to keep the upstream background under control, accounts for 40% loss in signal acceptance;

- the region of $m^2_{miss} > m^2_{\pi^0}$ between 35 and $40\,\mathrm{GeV}/c$ has a level of background comparable to or even better than the signal regions, albeit not included in the definition of signal.

Following these observations, a general re–optimization of the analysis has started, with focus on the:

- optimization of the definition of the signal regions;

- optimization of the particle identification;

- improvement of the cuts against the upstream background.

The following subsections detail the main modifications of the analysis implemented so far. Here the PNN analysis leading to the results described in sections 5.1 is referred as *standard*.
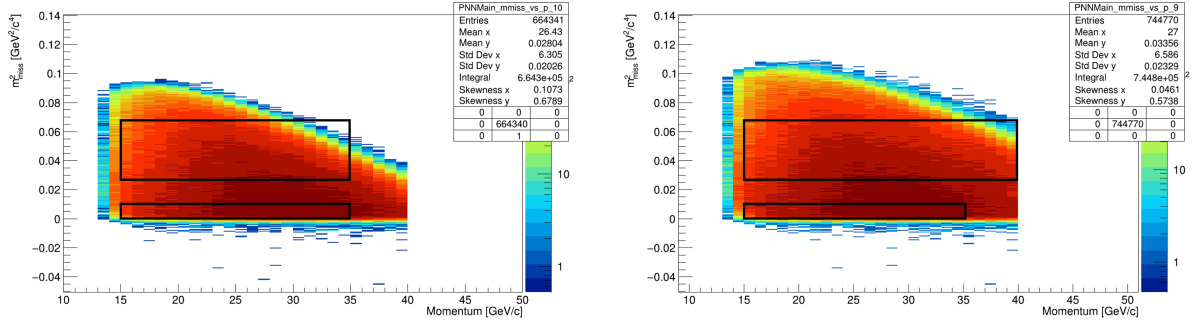
Figure 5: m_{miss}^2 versus π^+ momentum of simulated $K^+ \to \pi^+ \nu \bar{\nu}$ decays before (Left) and after (Right) the optimization of the signal region. The black boxes denote the two signal regions at low and high m_{miss}^2, that is Region 1 and 2, respectively.

5.2.1 Signal region definition

The first step of the analysis optimization is the removal of the kinematic conditions to reject $K^+ \to \pi^+ \pi^+ \pi^-$ decays. As a result this background increases by a factor 2, but still remains marginal overall, as evident from the outcome of the standard 2017 analysis. The $K^+ \to \pi^+ \nu \bar{\nu}$ acceptance, instead, increases in particular for events with $m_{miss}^2 > m_{\pi^0}^2$ and π^+ momentum above $35\,\mathrm{GeV}/c$, not included in the definition of the signal of the standard analysis. As a consequence, the above modification of the selection opens the possibility to extend the signal region above $35\,\mathrm{GeV}/c$. The option of expanding Region 2 up to $40\,\mathrm{GeV}/c$ has been investigated in detail. Figure 5 shows the signal regions definition before (left) and after (right) the modifications. After these modifications, the overall increase of signal acceptance is a factor 1.3. The $K^+ \to \mu^+ \nu$ background makes the extension of Region 1 above $35\,\mathrm{GeV}/c$ challenging. Studies are in progress in this respect.

5.2.2 $\pi^+ - \mu^+$ separation

The 2017 result show that the muon background in Region 2 is small enough to allow for an optimization of the $\pi^+ - \mu^+$ separation criteria, that accounts for about 35% loss of signal acceptance in the standard analysis. The most effective approach is to soften the cuts both on the calorimetric BDT classifier and on the RICH likelihood discriminant for events in Region 2. The new particle identification criteria lead to an increase of the signal acceptance in Region 2 by about 1.15. These modifications do not impact significantly on the background in this region, even if the muon rejection efficiency worsens by a factor 4. However the $K^+ \to \mu^+ \nu$ background prevents softening the $\pi^+ - \mu^+$ separation in Region 1. Therefore the overall increase of signal acceptance is about 1.1 when both Regions 1 and 2 are considered together.

5.2.3 Improved analysis of the 2017 data

In order to investigate the effects of the optimization, the 2017 data have been re-analysed with the proposed improvements. Table 2 summarizes the preliminary results from a re–analysis of the 2017 data that includes the above improvements, and a comparison with the standard analysis. The signal increases by a factor 1.43 while the background by 1.47. The $K^+ \to \pi^+ \pi^0$ background increases less than the signal because the π^0 rejection is optimal also in the $35-40\,\mathrm{GeV}/c$ region, while the bulk of this background stems from the region below $20\,\mathrm{GeV}/c$. A similar argument

Table 2: Expected number of SM signal and background events in signal region from 2017 data before and after the optimization of the $K^+ \to \pi^+ \nu \bar{\nu}$ analysis. The tilde in front of some of the estimated background after optimization means that the uncertainty are of the same order to that before optimization, albeit not yet studied in detail.

Process	2017 standard analysis	2017 optimized analysis
$K^+ \to \pi^+ \nu \bar{\nu}$ (SM)	$2.16 \pm 0.13_{syst} \pm 0.26_{ext}$	3.1 ± 0.4
$K^+ \to \pi^+ \pi^0(\gamma)$	$0.29 \pm 0.03_{stat} \pm 0.03_{syst}$	~ 0.33
$K^+ \to \mu^+ \nu(\gamma)$	$0.15 \pm 0.02_{stat} \pm 0.04_{syst}$	~ 0.15
$K^+ \to \pi^+ \pi^- e^+ \nu$	$0.12 \pm 0.05_{stat} \pm 0.06_{syst}$	~ 0.3
$K^+ \to \pi^+ \pi^+ \pi^-$	$0.008 \pm 0.008_{syst}$	~ 0.02
Upstream events	$0.9 \pm 0.2_{stat} \pm 0.2_{syst}$	1.4 ± 0.3
Total background	$1.5 \pm 0.2_{stat} \pm 0.2_{syst}$	2.2 ± 0.3

holds for the $K^+ \to \mu^+ \nu$ decay, because the corresponding background is all in Region 1, that has not been modified. The $K^+ \to \pi^+ \pi^- e^+ \nu$ background is estimated using MonteCarlo; the observed increases with respect to 2017 is due to the softening of the kinematic cuts against the $K^+ \to \pi^+ \pi^+ \pi^-$. The increase of the upstream background is comparable to that of the signal. The systematic uncertainty assigned to the upstream background is fully correlated between the standard and modified analysis, while the uncorrelated statistical uncertainty is about 10%. In addition, the upstream background has been investigated in detail, studying the control samples used to validate the estimation, as done in the standard 2017 analysis. A good agreement between the number of observed and expected upstream events is found in all the control data samples, showing no downside effect from the addition of the $35 - 40\,\mathrm{GeV}/c\ \pi^+$ momentum region.

5.3 Preliminary analysis of the 2018 data

The modified selection described in section 5.2 has been applied to the data taken in 2018 and reprocessed in 2019. All data collected until June 2018 suffered for a lack of shielding against hadrons originating upstream. This affects the 2016 and 2017 analyses and the data taken in the first 2 months of 2018. To keep the upstream background below the signal, the analysis of these data require a geometrical cut to avoid the regions without shielding. For this purpose, the π^+'s track is projected back to the surface of the final collimator and the event is rejected if the projection's position is within $|x| < 100\,\mathrm{mm}$ and $|y| < 500\,\mathrm{mm}$ (Fig. 6 left). From June 2018 onwards the installation of a new final collimator has fixed this issue. This allows the cut to be reduced to $|x| < 100\,\mathrm{mm}$ and $|y| < 100\,\mathrm{mm}$ (Fig. 6 right). The cut cannot be completely removed, as the beam hole of the collimator is anyway an unavoidable source of upstream events. The new condition against upstream background increases the signal acceptance by a factor 1.45 with respect to the standard analysis. As a result, the optimised analysis allows for an overall increment of the signal by a factor 2. However the net improvement is smaller, as the modifications of the selection against upstream background can be applied only to the data taken after June 2018, corresponding to about 78% of the total 2018 data.

Table 3 shows the preliminary expected number of background and SM signal events for the
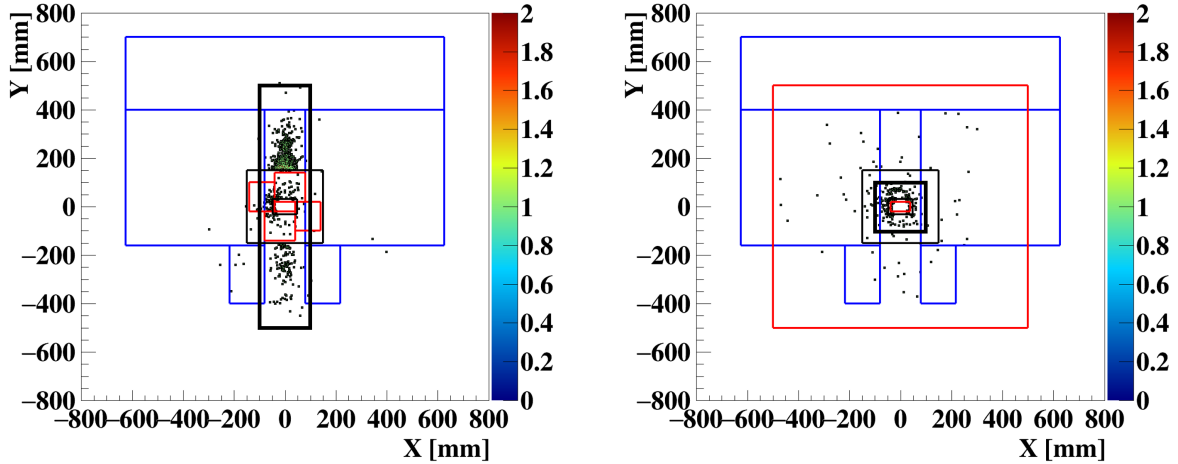
Figure 6: Position of the reconstructed π^+ projected at the final collimator for events passing a signal–like selection enriched in upstream events. The data shown are from 2017 (Left) and after June 2018 (Right). The central black thick box displays the geometrical cut that rejects the events inside. The blue contour is the transverse profile of the last dipole of the achromat. The red contours correspond to the shape of the final collimators employed in 2017 (Left) and 2018 (Right). The lighter black box shows the acceptance of the CHANTI detector that is effective against upstream events.

optimised $K^+ \to \pi^+ \nu \bar{\nu}$ analysis of the 2018 data. The signal expected is about three times more than that in the standard 2017 analysis. In total, 1.8 times more data have been collected in 2018 than in 2017. The analysis optimisation leads to an increase of the signal acceptance by about 1.8, compared with the standard analysis. This would give 7 signal events expected in 2018. However data in 2018 have been taken at an intensity about 10% higher intensity than in 2017. This causes about 5-10% additional signal loss, shared between a higher random veto efficiency and fraction of bursts rejected by data quality requirements and lower trigger efficiency.

All the background from K^+ decays scale as expected with respect to the 2017 data analysis The upstream background is still under study; preliminary results show that also this background scales linearly with the signal.

In conclusion, the analysis optimization in 2018 increases the signal acceptance by a factor of almost 2, while keeping the signal–over–background ratio similar to that of the standard analysis. This is in line with what was anticipated in the Addendum. The beamline configuration and the addition of the veto–counter system in 2021 aim to reduce the upstream background significantly, thus increasing the signal–over–background ratio.

5.4   Towards a full optimization

The global optimisation of the analysis is still in progress, focusing mainly on three topics:

1. rejection of the upstream background,

2. improvement of the $K^+ - \pi^+$ matching,

3. reduction of the random veto.

Table 3: Preliminary expected number of background events in signal region from 2018 data after the optimization of the $K^+ \to \pi^+\nu\bar{\nu}$ analysis. The first uncertainty on the number of expected SM signal events comes from the accuracy of the single event sensitivity, the second one is the theoretical error on the SM branching ratio.

Process	2018 analysis
$K^+ \to \pi^+\nu\bar{\nu}$ (SM)	$6.4 \pm 0.4_{syst} \pm 0.8_{ext}$
$K^+ \to \pi^+\pi^0(\gamma)$	0.6 ± 0.1
$K^+ \to \mu^+\nu(\gamma)$	0.3 ± 0.1
$K^+ \to \pi^+\pi^-e^+\nu$	0.5 ± 0.1
$K^+ \to \pi^+\pi^+\pi^-$	~ 0.04
Upstream events	Under study

A more general approach to reject the upstream background is under study using a multivariate analysis. To this purpose a Boost Decision Tree (BDT) classifier is built upon: the x, y position of the π^+ as projected back to the final collimator; the x, y position of the π^+ as projected to the first straw chamber; the slopes of the π^+ in the xz and yz planes; the x, y, z position of the reconstructed vertex. The simulation provides the training sample for the signal. Data from 2018 enriched in upstream events are used to model the background: this sample requires a tight signal–like selection necessary to pin down the features of the dangerous upstream events, and its limited size makes the training of the BDT difficult. Preliminary results suggest that this approach gives an increase of signal acceptance up to a factor 1.1 with respect to the cuts used so far, but the upstream background remains at the level of the improved cut–based analysis. However studies are on–going to better understand the effect of the BDT on the overall background and the interplay with the methods used for its evaluation. This approach is not yet part of the optimised analysis.

A refinement of the $K^+ - \pi^+$ matching algorithm offers a further possibility to increase the signal acceptance. Studies are on–going to improve the likelihood method used so far by a better choice of the likelihood functions. A more radical approach is also under investigation, replacing the likelihood with a supervised neural network. Both options show an increase of the signal acceptance by a factor 1.05–1.1, while keeping the same level of background from K^+ decays. The analysis is in progress to understand the impact on the upstream background. Presently the analysis still makes use of the standard likelihood method for $K^+ - \pi^+$ matching.

The third direction of improvement is the reduction of the random veto, i.e. the probability to lose signal events as a consequence of the photon and multiplicity rejection because of the accidental activity in the veto detectors. The random veto accounts for about 36% loss of the single event sensitivity in both the standard and optimised 2017 analyses and about 42% in the 2018 analysis. A reduction of the random veto is needed to make the future analysis more resilient to the beam intensity, and to improve the present signal efficiency. So far the approach taken is to reduce the various components of the random veto separately:

1. optimize the photon rejection algorithm with the LAV detector,

2. develop a LKr reconstruction specifically optimised for veto purposes,

3. refine the reconstruction of the small angle calorimeters IRC and SAC,

4. optimise the multiplicity rejection algorithm.

The work to reduce the LAV random veto is advanced and could be applied to the analysis of 2018 data. Details of this study are given in section 5.4.1.

The study of the photon rejection in LKr, IRC and SAC has started. In particular the treatment of the accidental clusters in LKr overlapped in space with photons from K^+ decays is challenging and requires a full reworking of the LKr reconstruction.

The multiplicity rejection accounts for about half of the overall random veto inefficiency in 2017. An important source of signal loss comes from the rejection of the segments reconstructed in the STRAW. The segments are tracklets formed by hits in the first and second, or third and fourth, chambers that match the decay vertex in space. A new algorithm has been developed with respect to that used by the standard 2017 analysis. Preliminary results show a reduction of the random veto of a factor 1.05 that directly translates into an equivalent increase of signal efficiency, while $K^+ \to \pi^+\pi^0$, $K^+ \to \pi^+\pi^+\pi^-$ and $K^+ \to \pi^+\pi^-e^+\nu$ backgrounds do not increase significantly. Additional checks are still on–going, but this improvement could be applied to the 2018 data analysis.

5.4.1 LAV random veto reduction with multivariate analysis

A data-driven multivariate analysis making use of the boosted decision tree (BDT) method has been developed to reduce the LAV random veto rate. The aim of the multivariate analysis is to discriminate real photon signals in the LAV blocks from muon halo signals. The entire 2017 data sample has been used to train and test the BDT and to evaluate the performace of the new LAV veto algorithm on the PNN selection.

An enriched photon sample has been obtained from PNN-triggered data using the PNN analysis selection with photon vetoes applied in all calorimeters except the LAVs.

The random veto sample has been obtained from a $K_{\mu2}$ event selection applied to control-triggered data in which the LAV veto in the L1 trigger is simulated. No photons are expected to be present in this sample, and the simulation of the L1 trigger LAV veto guarantees that random hits in the LAVs have the same characteristics expected in the PNN-triggered events.

In contrast to how the LAV veto was applied in the past, hits in LAVs upstream of the position of the reconstructed track vertex are ignored. The veto is based only on hits in detectors downstream of the vertex that are inside the veto time window (within ± 3 ns of the track time).

It is useful to distinguish among events with a single LAV hit, two LAV hits, or more than two LAV hits. For the photon sample, the majority of the events (57%) have two LAV hits. In 98% of these events, the two hits are in the same LAV and are close together in azimuth. Events with a single LAV hit account for 27% of the photon sample. For the random veto sample, events with a single LAV hit dominate (85%), and events with two hits account for only 10% of the sample. Events with more than two LAV hits make up the remaining cases. These events are always vetoed.

Two different BDTs have been built to discriminate between the photon (background) and random veto (signal) samples:

- BDT1 is for events with individual LAV hits in time. The input variables are the distance in time between the hit and the reconstructed track, the time-over-threshold measurements for the hit (for low and high thresholds), the edge mask indicating which threshold values were crossed on the leading and trailing edges of the signal, the LAV station and layer IDs, and the distance along the beam axis between LAV hit and the reconstructed decay vertex.

- BDT2 is for events with two hits in time in the same LAV with $\Delta\phi < 15°$. The two hits are clusterized to create the input variables: the number of layers between the two hits, the

17
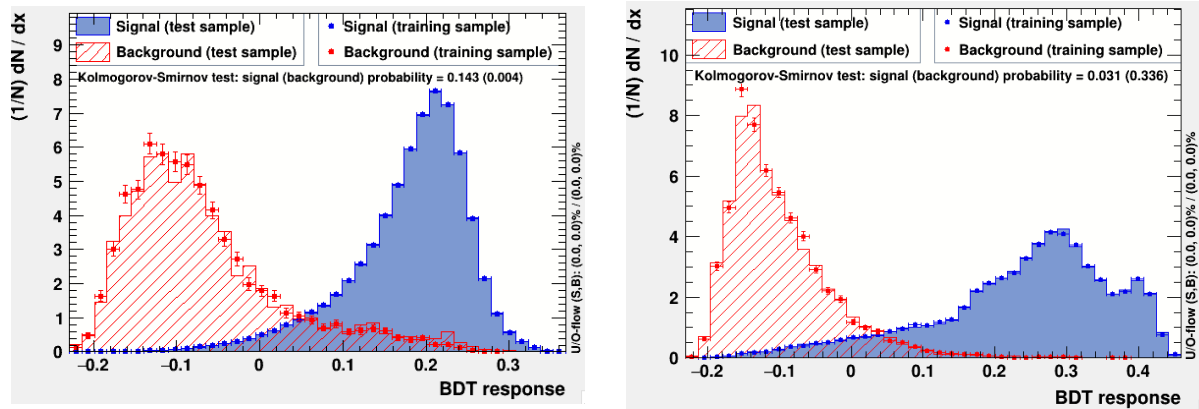
Figure 7: Left: BDT1 (one LAV hit in time) output. Right: BDT2 (two LAV hits in time on the same LAV and close together in azimuth) output. Random veto signal in blue, photon background in red.

difference in time between the two hits, the difference between the mean time for the two hits and the time for the track, the distance along beam axis between the mean position of the two hits and the reconstructed vertex, the sum of the times over threshold.

For events with two hits in different LAVs, or in the same LAVs with $\Delta\phi > 15$, the hits are separately entered into BDT1.

The BDT outputs obtained with about 80% of all 2017 data are shown in Figure 7. The red distributions are for photon hits; the blue distributions are for random veto hits. The remaining 20% of 2017 data has been used to test the discrimination power of the multivariate analysis.

The new LAV veto algorithm is based on cuts on the BDT1 and BDT2 output values with only hits in-time and downstream of the reconstructed vertex used to obtain the BDT output. Five different combinations of cuts on the BDT1 and BDT2 output values have been tested to optimize the photon rejection while maximizing the random veto efficiency. To calculate the π^0 rejection power, the new LAV veto algorithm is applied to the PNN sample selection for events with invariant mass in the $\pi^+\pi^0$ peak. To calculate the random veto efficiency, the algorithm is applied to the $K_{\mu 2}$ sample. The five cut combinations and the corresponding results for the π^0 rejection and random veto efficiency are listed in Table 4 and illustrated in Figure 8. The result is very promising: although the random veto inefficiency from the LAV veto in the L1 trigger cannot be recovered, the random veto inefficiency from the offline cuts can be reduced from 6% (2017 data analysis) to around 1%. The total background expectation for the different configurations is under evaluation and will allow optimization of the BDT cuts.

6 Rare and forbidden decays

A number of pre-scaled auxiliary trigger chains operating along with the main $K^+ \to \pi^+\nu\bar{\nu}$ trigger allow for a broad rare decay physics programme. Multi-track L0 triggers for collection of K^+ decays to lepton pairs (i.e. di-muon, di-electron and muon-electron pairs) are based on RICH and CHOD multiplicity requirements, as well as the total LKr energy deposit and MUV3 signal multiplicity conditions. The corresponding L1 trigger performs beam kaon identification by the KTAG and online reconstruction of a negatively charged track in the spectrometer. The data set collected in 2016–18 with the di-muon trigger is equivalent to 3×10^{12} kaon decays in
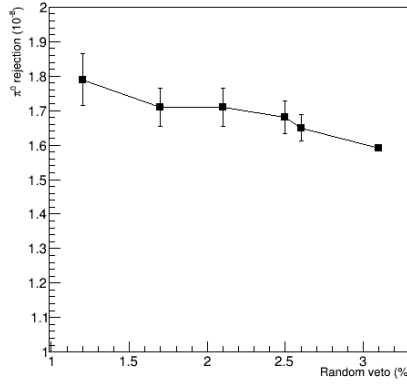
Figure 8: π^0 rejection versus random veto inefficiency for different combinations of BDT cuts.

Table 4: Random veto and π^0 rejection values for different combinations of BDT cuts

BDT cuts	Random Veto	π^0 rejection
BDT1 > 0.18 & BDT2 > 0.12	1.2%	1.65×10^{-8}
BDT1 > 0.20 & BDT2 > 0.14	1.7%	1.68×10^{-8}
BDT1 > 0.22 & BDT2 > 0.16	2.1%	1.71×10^{-8}
BDT1 > 0.24 & BDT2 > 0.18	2.5%	1.71×10^{-8}
BDT1 > 0.26 & BDT2 > 0.20	2.6%	1.79×10^{-8}

the vacuum tank upstream of STRAW1, while the data sets collected with the di-electron and electron-muon triggers are each equivalent to 10^{12} kaon decays. Additional data sets collected with a minimum bias trigger provided by the CHOD, and a non-muon trigger based on RICH and CHOD multiplicity with a MUV3 veto condition, both downscaled by factors of $\mathcal{O}(100)$, are equivalent to over 10^{10} kaon decays.

The record kaon flux is complemented by the excellent resolution on kinematic variables, particle identification and photon veto capabilities of the NA62 detector, leading to favourable background conditions. Measurements of various kaon and pion decays listed below are in progress and are in most cases based on the world's largest samples of these decays. Significant efforts go into the validation and improvement of the simulation of the detector response, aiming to understand and reduce the systematic uncertainties on these measurements.

A new measurement of the helicity-suppressed ratio $\Gamma(K^+ \to e^+\nu)/\Gamma(K^+ \to \mu^+\nu)$ [10] aims to improve on the sub-percent precision of the current best measurement [11] which would provide an important test of lepton flavour universality. The main trigger stream is used in the analysis, and the collected sample of $K^+ \to e^+\nu$ decays is several times larger than in the best measurement.

The flavour-changing neutral current decay $K^+ \to \pi^+\mu^+\mu^-$ [12] is under study. A new measurement of the decay rate and form factor parameters uses the di-muon trigger and the data sample is about 10 times larger than in the current best measurement [13]. The analysis will

also provide a test of lepton flavour universality by comparing the results to the $K^+ \to \pi^+ e^+ e^-$ measurements [14, 15]. Results from several ongoing analyses will test predictions of the Chiral Perturbation Theory describing low energy weak processes. These include the rare $K^+ \to \pi^+ \gamma\gamma$ decay [16] and the radiative decays $K^+ \to e^+ \nu\gamma$ and $K^+ \to \pi^0 e^+ \nu\gamma$ [17, 18] recorded by the pre-scaled control and non-muon triggers, as well as the $K^+ \to \pi^+ \pi^+ \pi^- \gamma$ [20], $K^+ \to \pi^+ \gamma e^+ e^-$ [19] and $K^+ \to \ell_1^+ \nu\ell_2^+ \ell_2^-$ (with $\ell_{1,2} = e, \mu$) [17] decays recorded with the multi-track trigger and lepton pair triggers. The data sample collected contains statistics which is larger than the currently most precise measurements for all of the listed decay channels [21, 22, 23, 24, 25].

Studies of neutral pion decays $\pi^0 \to e^+ e^-$ and $\pi^0 \to e^+ e^- \gamma$ and are also in progress. Both decays proceed via the same $\pi^0 \to \gamma^\star\gamma^\star$ vertex, described by the transition form factor entering the computations of the hadronic light-by-light scattering that contributes to the muon anomalous magnetic moment [26]. The measurement of the $\pi^0 \to e^+ e^-$ decay aims to resolve the existing 2σ tension between the SM theoretical prediction [27] and the latest experimental result [28]. The $\pi^0 \to e^+ e^- \gamma$ analysis aims to improve the measurements of the decay rate and the form factor slope [29].

Physics beyond the SM is also being explored: searches for K^+ decays forbidden in the SM, resonances in multi-body K^+ decays (which can be interpreted in terms of dark vector, dark scalar or axion emission [30, 31, 32]), and heavy neutral lepton production [33] in K^+ decays are being performed at record levels of sensitivity.

The collaboration has recently published new upper limits on the rates of the $K^+ \to \pi^- e^+ e^+$ and $K^+ \to \pi^- \mu^+ \mu^+$ decays based on about 30% of the data collected in 2016–2018 [34]. These processes violate conservation of lepton number by two units, and may be mediated by a massive Majorana neutrino [35, 36]. The limits obtained at 90% CL on the branching fractions are:

$$\begin{aligned}
\mathcal{B}(K^+ \to \pi^- e^+ e^+) &< 2.2 \times 10^{-10}, \\
\mathcal{B}(K^+ \to \pi^- \mu^+ \mu^+) &< 4.2 \times 10^{-11},
\end{aligned}$$

improving on the pre-NA62 searches by factors of 3 and 2, respectively. The reconstructed invariant mass spectra for the $K^+ \to \pi^+ \mu^+ \mu^-$ and $K^+ \to \pi^- \mu^+ \mu^+$ and processes obtained within this analysis are displayed in Fig. 9.

Searches for the above processes and other K^+ decays violating lepton number and flavour conservation using the complete 2016–18 data set are in progress. These searches are not limited by backgrounds, and the preliminary estimates of single event sensitivities for the 2017 data set are as follows: 5×10^{-11} for the $K^+ \to \pi^- \mu^+ e^+$ and $K^+ \to \pi^+ \mu^- e^+$ decays (improving by a factor of about 5 on the previous searches); 5×10^{-11} for the $K^+ \to e^- \nu\mu^+ \mu^+$ decay (which is the first search for this mode), and 10^{-10} for the $K^+ \to e^- \nu e^+ e^+$ decay (factor 100 improvement on the PDG).

The collaboration presented new results for the search of heavy neutral lepton (N) production in $K^+ \to e^+ N$ and $K^+ \to \mu^+ N$ decays with about 30% of the 2016–18 data set at the Kaon conference in September 2019. The model-independent upper limits obtained on the lepton mixing parameters $|U_{e4}|^2$ and $|U_{\mu4}|^2$ improve by two orders of magnitude over those obtained from the analysis of the pilot data set collected in five days of operation in 2015 without the GTK detector [37]. The limits obtained on the $|U_{e4}|^2$ parameter improve on the existing limits from production decay searches in the mass range accessible [38], and saturate the range allowed by the Big Bang Nucleosynthesis constraint [39] up to the HNL mass of 300 MeV/c^2. The preliminary results first presented in 2019 are shown in Fig. 10. Publications based on the complete 2016–2018 data set are in preparation.
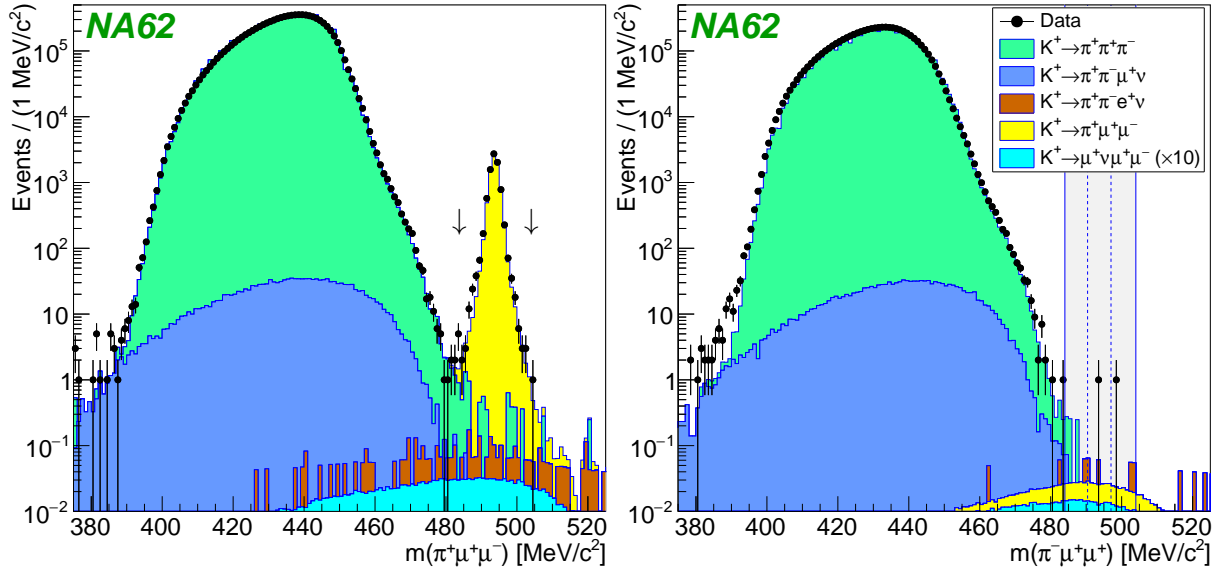
Figure 9: Reconstructed mass spectra of the SM $\pi^+\mu^+\mu^-$ (left) and LNV $\pi^-\mu^+\mu^+$ (right) final states obtained with 30% of the data set collected so far [34]. Data spectra are overlayed with background estimates based on simulations. The shaded vertical band indicates the region masked during the analysis, including the LNV signal region bounded by dashed lines.
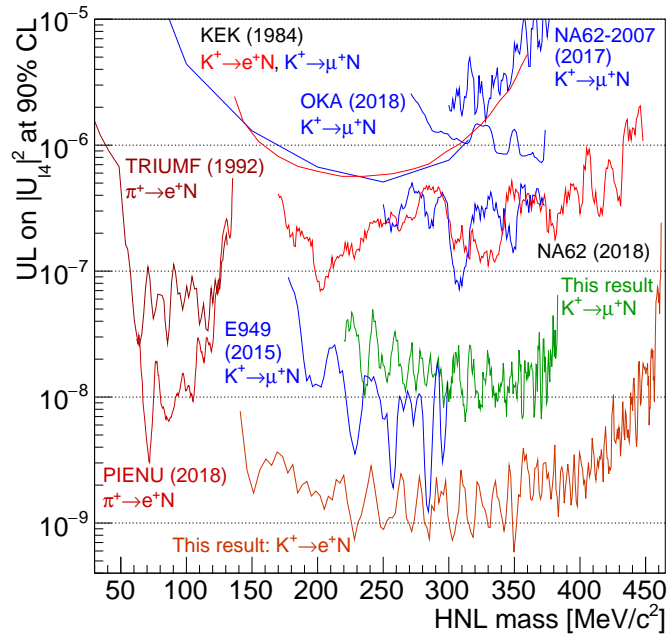
Figure 10: Upper limits at 90% CL on the heavy neutral lepton mixing parameters $|U_{e4}|^2$ and $|U_{\mu4}|^2$ obtained from a production search with a partial (30%) NA62 data set for each assumed HNL mass compared to the limits established by earlier HNL production searches in $K^+ \to e^+N$ and $\pi^+ \to e^+N$ decays.

7 Exotic processes

Thanks to its high intensity beam and detector performance (redundant particle-identification capability, extremely efficient veto system and high resolution measurements of momentum, time, and energy), NA62 can achieve sensitivities to long-lived light mediators in a variety of new-physics scenarios. Long-lived mediators faintly coupled to the SM fields can be produced in meson decays from proton interactions, and can reach the decay volume decaying therein. If charged particles are produced as decay products, as is the case for dark photons and heavy neutral leptons, the standard signature would be the identification of a decay vertex from two oppositely charged tracks, spatially displaced from the beam line, and (for two body modes) corresponding to the mass of the new mediator. If photons are produced, as is the case for certain models of axion-like particles (ALPs), the signature consists in two photon clusters in the LKr in absence of charged particles activity, with a peculiar distribution of the total energy and photon-photon barycenter position, resembling the dynamics of the ALP emission.

Such scenarios are under test using data taken in 2016–2018. Short dedicated runs were collected, in which the beryllium target was lifted and the proton beam was dumped after closing the movable beam-defining collimator (TAX), almost 20 m downstream the target. In addition, dedicated low-bandwidth triggers were implemented in parallel to the standard data taking, to select samples with pair of charged particles in the final state. A summary of the data collected, expressed in total number of protons on target (POT) is reported in Table 5.

Configuration	Statistics available, POT	Trigger
Beam dump	2.9×10^{16}	Two tracks
Beam dump	2.6×10^{16}	> 3 GeV deposited in LKr
Standard	8×10^{17}	Di-muon
Standard	2×10^{17}	Pion-muon

Table 5: Summary of data taken in 2016–2018 to be used for searches for long-lived new-physics exotic states.

Preliminary results from the ongoing analyses indicate that the background does not limit the sensitivity with the present data set. Sensitivity studies to extrapolate to 10^{18} POT show that a large fraction of the background events are due to charged particles produced upstream of the fiducial volume. The ANTI0 hodoscope will be installed for the next data taking at the entrance of the fiducial volume, to limit this background. The hodoscope has been designed to give a rejection factor of 10^3 for each charged particle due to upstream-generated background.

7.1 Search for a long-lived ALP in the π^0 mass region

A high-sensitivity search for π^0 decays into invisible particles is a natural by-product of the search for the ultra-rare decay $K^+ \to \pi^+ \nu \bar{\nu}$.

The decay $\pi^0 \to \nu \bar{\nu}$ has been of historical interest for the study of neutrino properties such as mass, helicity and number of families, and is forbidden for pure left-handed massless neutrinos due to angular momentum conservation. The observation of neutrino oscillations demonstrated non-zero neutrino masses, thus allowing the $\pi^0 \to \nu \bar{\nu}$ decay within the Weak interaction. Since cosmological arguments constrain the sum of the neutrino masses to well below 1 eV/c^2, the upper limit on BR($\pi^0 \to \nu \bar{\nu}$) is $O(10^{-24})$, well below the experimental sensitivity. The present experimental limit is 2.7×10^{-7} at 90% CL [40]. Therefore the present interest in the search for π^0 decaying to any invisible final state ($\pi^0 \to$ invisible in the following) is in testing new-physics scenarios involving feebly-interacting or long-lived particles. Any observation of $\pi^0 \to$ invisible at the present sensitivity would be a clear indication of new physics beyond the SM.

The search for $\pi^0 \to$ invisible is performed with the decay chain

$$K^+ \to \pi^+\pi^0(\gamma), \quad \pi^0 \to \text{invisible}, \qquad (2)$$

inclusive of radiative corrections to the K^+ decay. Stringent requirements are applied to $\pi\nu\bar{\nu}$-trigger data to reject events with any additional activity correlated in time to the incoming K^+ and its daughter π^+. The branching ratio for $\pi^0 \to$ invisible is computed as:

$$\text{BR}(\pi^0 \to \text{invisible}) = \text{BR}(\pi^0 \to \gamma\gamma) \times \frac{N_{\text{s}}}{N_{\pi^0} \times \epsilon_{\text{sel}} \times \epsilon_{\text{trig}}}, \qquad (3)$$

where N_{s} is the number of signal events, obtained after background subtraction from the observed event counts; ϵ_{sel} and ϵ_{trig} are the efficiency corrections due to the signal-selection algorithm and the $\pi\nu\bar{\nu}$ trigger, respectively, and N_{π^0} is the the number of tagged π^0 mesons selected from control-trigger data and used for normalization (exactly as for the analysis of $K^+ \to \pi^+\nu\bar{\nu}$).

After the signal-sample selection, the residual background is dominated by $K^+ \to \pi^+\pi^0(\gamma)$ events with $\pi^0 \to \gamma\gamma$ where all the photons are undetected. To estimate the expected background, an *a-priori* knowledge of the background rejection power is obtained from a combination of data-based studies and Monte Carlo (MC) simulations. The single-photon efficiency of the sub-detectors forming the photon-veto system are evaluated using control-trigger data and MC simulation samples. Using a $K^+ \to \pi^+\pi^0(\gamma)$ simulated sample, the detector efficiencies are evaluated and combined to estimate the expected background rejection, which strongly depends on the π^+ momentum (Figure 11).
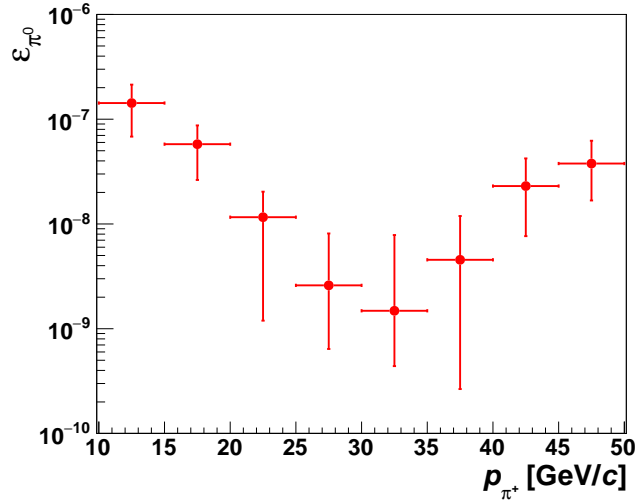
Figure 11: *Expected background rejection ε_{π^0} as a function of the charged pion momentum p_{π^+}.*

A blind analysis is performed in bins of the π^+ momentum. A momentum interval between 25 and 40 GeV/c is chosen to optimize the analysis sensitivity in the hypothesis of absence of signal, and the experimental inputs to Equation 3 are evaluated in this π^+ momentum range. For method validation, data sub-samples where no signal is expected from past searches for $\pi^0 \to$ invisible are compared to the expected background and systematic errors are derived.

In the selected sample of $\pi\nu\bar{\nu}$-trigger data, 12 events are observed in the π^+ momentum range 25–40 GeV/c out of 4 billion tagged π^0 mesons. The expected background amounts to 10^{+22}_{-8} events. The observed number of events is therefore compatible within the uncertainties

with a pure-background scenario. In Table 6, the number of observed events (N_{obs}) is compared to the expected background (N_{bkg}) in 5 GeV/c bins of the π^+ momentum. The CL$_{\mathrm{s}}$ method [7]

Table 6: *Number of expected background events and number of observed event counts in 5 GeV/c bins of the π^+ momentum.*

Momentum bin [GeV/c]	N_{bkg}	N_{obs}
25 − 30	$3.5^{+7.5}_{-2.7}$	3
30 − 35	$1.9^{+8.0}_{-1.3}$	6
35 − 40	$4.8^{+7.8}_{-4.5}$	3

is used to determine a frequentist 90% confidence interval for the number of signal events, which is $N_{\mathrm{s}} < 8.24$. From Equation 3, the upper limit on the branching ratio for $\pi^0 \to$ invisible is extracted:

$$\mathrm{BR}(\pi^0 \to \mathrm{invisible}) \leq 4.4 \times 10^{-9}. \tag{4}$$

This result improves on the previous most stringent upper limit [40] by a factor of about 60, and a paper is in preparation.

8   Publication of NA62 data

Since the last NA62 SPSC review in April 2019, the collaboration has completed the following publication:

- E. Cortina Gil et al. (NA62 collab.), Search for production of an invisible dark photon in π^0 decays, JHEP 05 (2019) 182.

- E. Cortina Gil et al. (NA62 collab.), Searches for lepton number violating K^+ decays, Phys. Lett. B797 (2019) 134794.

The paper on the result of the $K^+ \to \pi^+ \nu\nu$ analysis on 2017 data is about to be submitted for publication.

The collaboration is actively contributing to major International Conferences and topical Workshops with recently published or preliminary physics results from NA62 and NA48/2 data analyses. In the past year (May 2019 to April 2020), the collaboration speakers presented 42 plenary talks, 28 parallel talks and 5 posters to Physics Conferences, and 6 talks and 3 poster to Instrumentation Conferences. In particular, NA62 contributed with several results and presentations to the KAON2019 Conference. More contributions are already foreseen in future 2020 Conferences.

References

[1] E. Cortina Gil *et al.* (NA62 collab.), JINST 12 P05025 (2017).

[2] 2019 NA62 Status Report to the CERN, SPSC-SR-249.

[3] Report from the Conventional Beams Working Group to the Physics beyond Colliider Study and to the European Strategy for Particle Physics, CERN-PBC-REPORT-2018-002.

[4] R. Ammendola *et al.*, *Nucl. Instrum. Meth.* A **929** (2019) 001–022.

[5] M. Tanabashi *et al.*, (Particle Data Group), *Phys. Rev.* D **98** (2018) no. 3 030001.

[6] E. Cortina Gil *et al.* (NA62 collab.), Phys. Lett. B **791** (2019) 156-166.

[7] A.L. Read, J. Phys. G **28** (2002) 2693.

[8] Y. Grossman and Y. Nir, Phys. Lett. B **398** (1997) 163.

[9] Addendum I to P326, SPSC-2019-039.

[10] V. Cirigliano and I. Rosell, Phys. Rev. Lett. **99** (2007) 231801.

[11] C. Lazzeroni *et al.* (NA62 collab.), Phys. Lett. **B719** (2013) 326.

[12] A. Crivellin *et al.*, Phys. Rev. **D93** (2016) 074038.

[13] J. R. Batley *et al.* (NA48/2 collab.), Phys. Lett., bf B697 (2011) 107.

[14] R. Appel *et al.*, Phys. Rev. Lett. **83** (1999) 4482.

[15] J. R. Batley *et al.* (NA48/2 collab.), Phys. Lett., **B677** (2009) 246.

[16] G. Ecker, A. Pich and E. de Rafael, Nucl. Phys. **B303** (1988) 665.

[17] J. Bijnens, G. Ecker, and J. Gasser, Nucl. Phys. **B396** (1993) 81.

[18] V. Cirigliano *et al.*, Rev. Mod. Phys. **84** (2012) 399.

[19] F. Gabbiani, Phys. Rev. **D59** (1999) 094022.

[20] G. D'Ambrosio *et al.*, Z. Phys. **C76** (1997) 301.

[21] J. R. Batley *et al.* (NA48/2 collab.), Phys. Lett., **B730** (2014) 141.

[22] C. Lazzeroni *et al.* (NA62 collab.), Phys. Lett. **B732** (2014) 65.

[23] F. Ambrosino *et al.* (KLOE collab.), Eur. Phys. J. **C64** (2009) 627.

[24] S. A. Akimenko *et al.* (ISTRA+ collab.), Phys. Atom. Nucl. **70** (2007) 702.

[25] M. M. Shapkin *et al.* (OKA collab.), Eur. Phys. J. **C79** (2019) 296.

[26] Muon $g-2$ Experiment, https://muon-g-2.fnal.gov/.

[27] T. Husek, K. Kampf and J. Novotný, Eur. Phys. J. **C74** (2014) 3010.

[28] E. Abouzaid *et al.*, Phys. Rev. **D75** (2007) 012004.

[29] C. Lazzeroni *et al.* (NA62 collab.), Phys. Lett. **B768** (2017), 38.

[30] F. Bezrukov and D. Gorbunov, JHEP **05** (2010) 010.

[31] D. Alves and N. Weiner, JHEP **07** (2018) 092.

[32] G. Krnjaic *et al.*, Phys. Rev. Lett. **124** (2020) 041802.

[33] L. Canetti *et al.*, Phys. Rev. **D87** (2013) 093006.

[34] E. Cortina Gil *et al.* (NA62 collab.), Phys. Lett. **B797** (2019) 134794.

[35] L. Littenberg and R. Shrock, Phys. Lett. **B491** (2000) 285.

[36] A. Atre *et al.*, JHEP **0905** (2009) 030.

[37] E. Cortina Gil *et al.* (NA62 collab.), Phys. Lett. **B778** (2018) 137.

[38] J. Beacham *et al.*, J. Phys. **G47** (2020) 010501.

[39] A. D. Dolgov *et al.*, Nucl. Phys. **B590** (2000) 562.

[40] A. V. Artamonov *et al.* (E949 Collaboration), Phys. Rev. D **72** (2005) 091102.

[41] M. J. Dolan, F. Kahlhoefer, C. McCabe and K. Schmidt-Hoberg, JHEP **1503** (2015) 171, Erratum: [JHEP **1507** (2015) 103].